Chapter 11

Noninvasive Methods for Condition Monitoring and Electrical Fault Diagnosis of Induction Motors

Muhammad Aman Sheikh, Nursyarizal Mohd Nor,

Taib Ibrahim, Sheikh Tahir Bakhsh,

Muhammad Irfan and Hanita Binti Daud

Additional information is available at the end of the chapter

http://dx.doi.org/10.5772/67245

Abstract

This chapter provides a comprehensive analysis of noninvasive methods to diagnose stator winding insulation faults of an induction motor. Further, a novel noninvasive method is proposed to diagnose the root cause of winding failure due to unbalanced voltage to avoid catastrophic failure. Therefore, a winding function approach is utilized to derive an analytical expression for stator winding distribution and magnetomotive force (MMF). This tactic qualifies the conductor segment that generates MMF, and it also helps to analyze a healthy current spectrum. One can easily observe higher order harmonics in current spectrum; therefore, a new series of rotor harmonics is introduced to diagnose unbalanced supply. The locus of these harmonics is dependent on the poles, rotor bars, and slip. Due to the rapid complexity in industrial plants, it is inconceivable to continue human inspection to diagnose the faults. Thus, to avoid human inspection, in addition to new series of rotor harmonic, a fully automatic method based on neural network is proposed. This method not only diagnoses unbalanced voltage but it also recognize the percentage of unbalanced voltage by use of feed-forward multilayer perceptron (MLP) trained by back propagation. Finally, the experimental results shows the validation of this research work proposed method.

Keywords: artificial neural network (ANN), diagnosis, fault detection, induction machine, interturn short circuit, rotor harmonic, unbalanced voltage

1. Introduction

Condition monitoring is of a great concern to ensure continue production, reliability, and consequently, avoid catastrophic failures. Therefore, online condition monitoring of induction motor has become a subject of interest and a challenging task for the protection of a motor [1, 2]. In induction motor, the most critical component, which is also considered the main source of motor failures, is stator winding insulation failure [3–6]. Over the last few decades, numerous surveys have been carried out on the reliability of induction motor. It has been experienced that 37% of motor failure is due to insulation breakdown.

It is found that unbalanced voltage is a major source of insulation breakdown. The unbalanced voltage results in an unscheduled shutdown of the process and causes enormous costs. Thus, it is desirable that the misalignment in the voltage source, which can result in a severe failure, should be identified at an incipient stage. A substantial amount of work has been proposed based on current and voltage [7], current residue, the phase shift in current and voltage [8], and sequence components [4, 9–11]. The majority of the methods to diagnose the unbalanced voltage essentially (invasive or noninvasive) monitor single or multiple indicators of stator faults. Most of the latter are extracted from a signature analysis. Therefore, it is important to be familiar with the spectrum of a healthy motor, which is a challenging task due to the complexity of electromagnetic processes, time, and space variables of an induction motor. Conversely, it is essential to have a mathematical modeling that enables to extract a geometrical representation of the motor. Beside this, to interpret the results from the mathematical model it is necessary to introduce an appropriate analytical model. The modeling of stator conductor segments and MMF is a most reliable approach to execute correct interpretation of induction motor.

As mentioned earlier that the unbalanced voltage is a major source of insulation breakdown, therefore, the aim of this paper is to diagnose this fault at an incipient stage. The unbalanced voltage can lead to turn-turn fault, phase-phase fault, phase-ground fault, and even a destructive effect on the stator core. During the last few decades, the condition monitoring of induction motor has become a vigorous area of research. Substantial work has been executed to propose and develop various techniques and methods to diagnosis motor faults. Through most relevant literature, three major classes of methods are discovered which support the task of fault monitoring [8]. The first class is based on a signal analysis [12, 13] that uses spectra in a frequency domain, time domain, time-frequency domain, and high-order harmonics. The second approach is based on analytical modeling [14] that involves mathematical models to measure input and output feature such as residuals, state estimation, and parameter estimation that incorporate the artificial intelligence (AI) to online automate analyze the health of induction motor through measured signals [15]. In engineering the AI tools are of great significance to solve various complex problems [16, 17]. The AIs are classified into four different groups as an expert system, genetic algorithm (GA), fuzzy logic, and artificial neural networks (ANNs) [18].

This paper aims to analyze the current spectrum of the induction motor to diagnose and distinguish between balanced and unbalanced voltage against the different level of unbalanced voltage. In the first part of the chapter, a comprehensive analysis of noninvasive methods is

http://dx.doi.org/10.5772/67245

presented to diagnose electrical faults. While in the second part, an analytical model is derived for the conductor segments, which are responsible for the generation of MMF. In third part, a reminiscence is carried out on MMF and an expression is derived to modify MMF with reference to the slot conductors that play an import role in the generation of MMF by introducing all harmonics terms that have influence in MMF waves. Further, a novel noninvasive technique based on ANN is presented in Section 6 along with results and test procedure to diagnose and distinguish unbalanced voltage at incipient stage in order to avoid catastrophic failure. Finally, conclusions and future work are presented in Section 7.

2. Noninvasive stator fault diagnosis methods

Diagnosis of stator winding insulation failure has been extensively studied. Some of the approaches are based on laboratory tests while other are based on experimental results and analysis through simulation. Mostly, the researchers divide the diagnosis techniques into two main categories, i.e., invasive and noninvasive. Although invasive fault diagnosis methods help to diagnose the defect but it has many drawbacks, some are mentioned as: most of the invasive techniques are offline or sensor bases, for installation of the sensors the normal operation of an induction motor is disturbed. Moreover, by influenced operation of contiguous equipment, there is no proper capability to diagnosis the weak faults. In contrast, noninvasive methods make use of stator current and voltage, or other important electrical quantities. There is no constraint of sensors to be installed. It is a cost-effective approach because in industries, current and voltages are usually measured, thus the economic cost of current and voltage measurement is not imposed on the system. Therefore, noninvasive methods in recent years are preferred over invasive. The next subsection describes the operating principle of noninvasive indexes of how the stator winding faults are diagnosed.

2.1. The air-gap torque

The air-gap torque between the stator winding and the rotor is induced by current and flux linkages that are sensitive to asymmetry caused by unbalanced voltage supply. The fault can be diagnosed by stator current and voltage. The motor with interturn short circuit will generate forward and backward rotational fields; the forward rotational field has a constant torque with correspondence to the motor rotating field, while the backward rotational field has twice the oscillating torque as compared to motor supplied frequency [19]. Therefore, the frequency of backward rotating field may be used as an interturn fault index. However, the induction motor with unbalanced three-phase voltages also accesses the same oscillating torque component. This index may be an expensive approach because it requires measuring both current and voltage. Moreover, this index cannot distinguish between interturn and unbalanced voltage.

2.2. The stator line current

The stator line current is the index that may be used to reflect a variety of noninvasive indexes to diagnose interturn fault. The stator line current indexes are briefly described in the succeeding

text. First, consider three current sequences positive, negative, and zero of a three phase as follows:

$$X^0 = \frac{1}{3}(X_a + X_b + X_c) \tag{1}$$

$$X^+ = \frac{1}{3}(X_a + aX_b + a^2X_c) \tag{2}$$

$$X^- = \frac{1}{3}(X_a + a^2X_b + aX_c) \tag{3}$$

where $a = e^{j2\pi/3}$. The healthy induction motor without any fault or symmetry has zero current for a negative sequence, whereas the interturn fault in motor generates considerable negative sequence current. While there is minute change observed for positive sequence current, there is no effect of load variation on the negative sequence current, but it is highly sensitive to the imbalance of the supply voltages and can easily inherent asymmetry [19]. Therefore, this index does not properly indicate the interturn fault and unbalanced voltage.

Park vector estimation, analysis uses the machine line current to diagnose interturn faults [20]. Under healthy condition, the motor Park vector pattern corresponds to a circular pattern. While in the occurrence of interturn short circuits, the Park vector pattern manifests to an elliptic representation and with the severity of fault the ellipticity increases. Through experiments and simulation results it has been proven that Park vector is a reliable approach to detect the interturn fault but does not investigate unbalanced voltage supply [20, 21].

In induction motor, the motor current signature analysis (MCSA) is the most extensively used diagnosis index [22, 23]. It is observed that current spectrum is also affected by unbalanced voltage supply. Thus, the current spectrum will have third-order harmonics under interturn as well as under unbalanced conditions. Therefore, MSCA is confused with the similar behavior of induction motor harmonics under faulty and unbalanced conditions. Hence, MCSA approach is not a reliable index to sufficiently identify the faults.

2.3. Power

The instantaneous electrical power is one of the reliable faults diagnose indexes for induction motor [24], and some of the power frequency components have been identified as the stator windings fault index [8]. Power frequencies are only dependent on the severity of the fault but independent of the speed. The major factor that makes this index less reliable is that it is influenced by peripheral factors such as inherent asymmetries, unbalanced supply voltage, measuring equipment, and load variations. It is an expensive fault index because this requires measurement of both voltage and current signals.

2.4. Sequence impedance matrix

Negative sequence apparent impedance is a noninvasive method and is used as a fault index to detect stator winding faults [25, 26]. The impedance is obtained through the phasor voltage

http://dx.doi.org/10.5772/67245

and phasor current. When interturn fault occurs, the impendence of the motor will be disturbed. In this way, the change in the impedance is an indication of the faulty motor. This index is less sensitive to load variation and unbalanced voltage. Therefore, it can be a preferable method to diagnose the interturn stator winding faults, but it is a bit expensive and lengthy approach because both the signal voltage and current have to be monitored.

2.5. Stator voltage

Stator voltage is also used as an index to detect the stator winding faults [27, 28]. By adopting this approach, the algebraic sum of three-phase voltages is useful because this approach relies on the variation of residual voltage caused by an interturn fault. For healthy motor, the residual voltage is zero, while it is nonzero for an interturn motor. In a real scenario even in the healthy induction motor, there are no balanced three-phase windings. Therefore, this index is less reliable under load conditions. In this method, machine voltage harmonics are observed by disconnecting the terminals [27], so this method cannot be applied for online condition monitoring. After disconnecting the voltage terminals, the odd harmonics of the motor are observed and used as interturn fault index [28].

From the above-mentioned methods, none of the methods is capable of distinguishing unbalanced voltage. Thus, to tackle unbalanced anomalies at the incipient stage all the three classes of conditioning monitoring techniques are implemented in this research to diagnose unbalanced voltage at incipient stage, i.e., signal analysis class, analytical modeling class, and knowledge-based class.

3. Analytical expression for spatially distributed stator winding

In induction motors, the armature winding is at the stator side between the stamped slots. **Figure 1** shows a stator with 12 slots and it can be illustrated that the winding in an induction motor is not a single coil but is composed of a number of coils that are spatially distributed and placed in the axial direction to provide room for the generation of magnetic flux.

Moreover, the stator winding of an induction motor is distributive in nature and can be elucidated either by a discrete or by a continuous formulation. The discrete description refers to the number of conductors in a slot while continue distribution is based on the density of the windings. However, the conductors of stator winding are not placed in a continuous manner, but rather are located in the slots. As the conductors have a physical size, which could be viewed with sufficient resolution, therefore, the stator winding can be described mathematically to derive an analytical expression for the conductor segments that are responsible for the generation of MMF that is the first task of proposed work and each slot is partition down to slot and end conductors as shown in **Figure 2**.

The main focus of this section is to derive an analytical model for the slot conductors that are oriented in axial direction. The reason to focus more on slot conductors is that these windings are the portion of stator conductor that establishes MMF and that is involved in the production of a torque. **Figure 1(a)** illustrates the stator of induction motor with 12 slots, whereas the

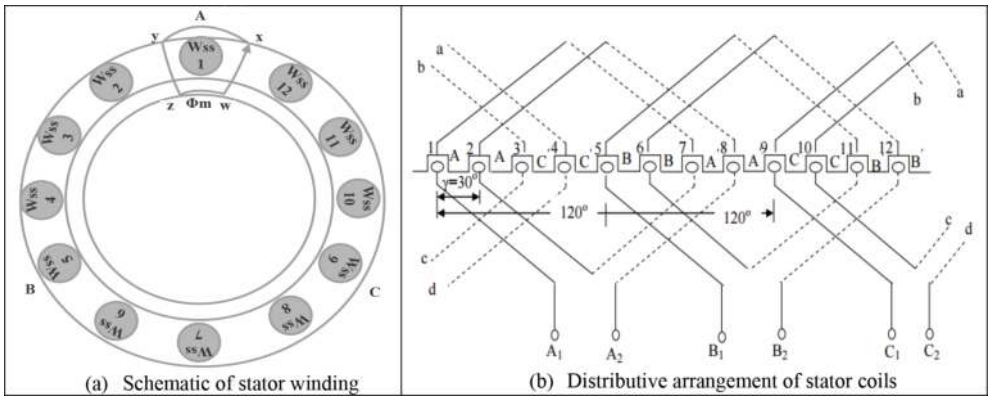

Figure 1. Stator winding arrangement in the slots.

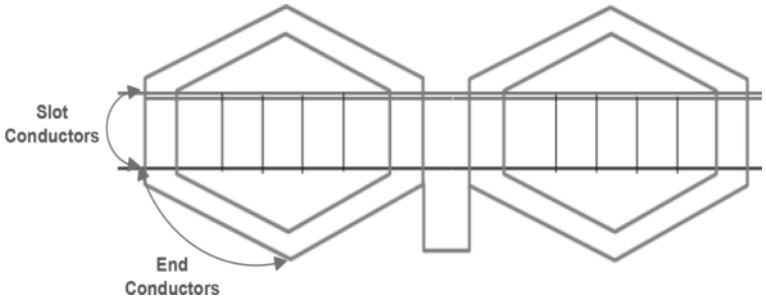

Figure 2. Partition of stator winding into slot and end conductions.

stator windings are located in each slot. The notation $W_{ss,i}$ indicates the conductors in the *i*th slot where "*as*" refer to phase-a of the stator winding. The conductors in the slots are shown as open circles. Subsequently, the notation can be used to derive an expression for the segment of slot conductors. For more generalize case, generalizing this notation, $W_{ss,i}$ is the conductors of any phase in slot *i*th of winding:

$$W_{ss} = \sum_{i=1}^{n} W_{ss,i} u(W_{ss,i}) \tag{4}$$

Figure 3 is a version of a developed diagram of the stator winding of induction motor. In this developed diagram, instead of front or back view of a machine, the angle of vision is from the center of a stator to outward. Within the slots, $W_{x,i}$ denotes the number of slot conductors of i^{th} *slot*. Where, W_{os} and W_{is} are the variables representing front end conductor directed to the left or right, respectively. It can be illustrated that for a symmetrical induction motor without any fault, these conductors are same in numbers as given in expression:

http://dx.doi.org/10.5772/67245

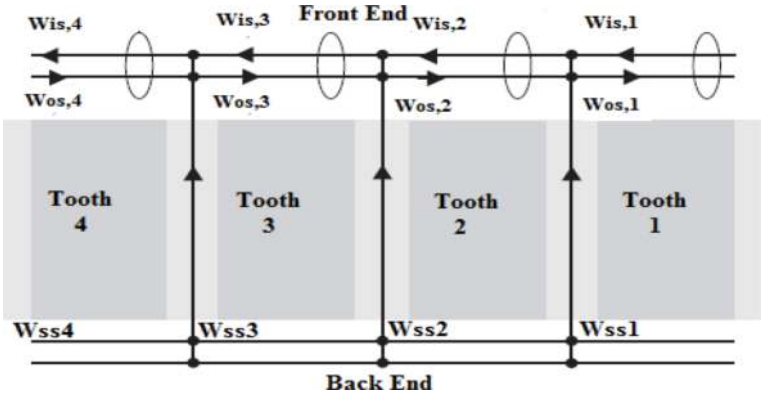

Figure 3. A version center view of stator through a developed diagram.

$$\sum_{i=1}^{n} Wo_{ss,i} u(W_{ss,i}) = \sum_{i=1}^{n} Wi_{ss,i} u(W_{ss,i}) \tag{5}$$

In most of the induction motors, the stator winding is multilayered that contains conductors from multiple windings (phases) as shown in **Figure 4**. Conductors out of the slot are known as end conductors and are of importance because they contribute to the inductance and resistance of the winding. Thus, total end conductors are given as in Eqs. (6)–(7).

$$E_{ss} = \sum_{i=1}^{n} Wo_{ss,i} + \sum_{i=1}^{n} Wi_{ss,i} \tag{6}$$

$$E_{ss} = \sum_{i=1}^{n} E_{ss,i} u(E_{ss,i}) \tag{7}$$

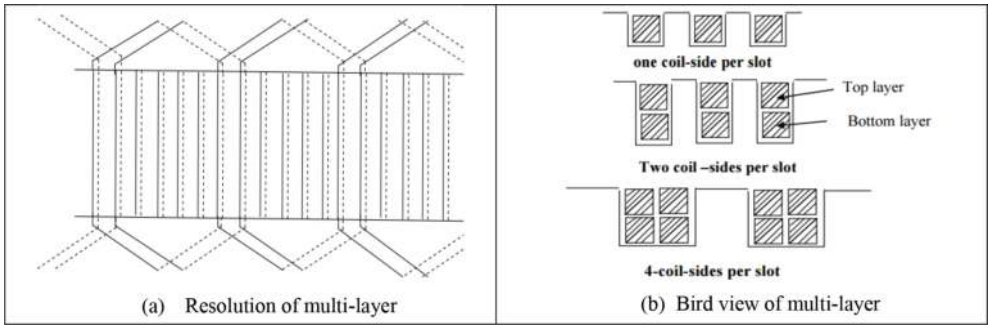

Figure 4. Multilayer stator winding. (a) Resolution of multilayer. (b) Bird view of multilayer.

As the stator winding is segmented into slot and end conductors, therefore the total number of turns associated with the winding will be the combination of slot conductors and end conductors:

$$W_T = \sum_{i=1}^{n} W_{ss,i} u(W_{ss,i}) + \sum_{i=1}^{n} E_{ss,i} u(E_{ss,i}) \tag{8}$$

Further, to calculate a center of stator teeth and stator slot, respectively, the following expression can be used based on the developed diagram:

$$\varnothing_{ss,i} = \frac{\pi(2i-2)}{T_s} + \varnothing_{ss,1} \tag{9}$$

$$\varnothing_{st,i} = \frac{\pi(2i-3)}{T_s} + \varnothing_{ss,1} \tag{10}$$

where T_s represents total stator slots, while $\varnothing_{ss}$ and $\varnothing_{st}$ represent the center of slot and teeth, respectively.

4. Analytical derivation of stator and rotor MMF with reference to modified slot conductors

4.1. Analytical expression of stator MMF

In induction motors, the primary goal of windings is to produce a rotating MMF. Therefore, the windings of induction motors are designed in such a way that the induced EMF or produced MMF consists predominantly of the space-fundamental sinusoidal component. The phase windings of an induction motor are identical but distributed and shifted in space for $2\pi/3p$. The winding of each phase occupies one-third of the number of the total slots in an axial direction. The regions of stator winding within the slot known as slot conductors are of great importance because these are the portions of stator conductor that establish MMF and that are involved in the production of torque. The stator MMF is given as [29]

$$F_{ss}(t,\theta) = \sum\nolimits_{\mu} M_{\mu} \cos(\omega t - \mu p\theta)\ ;\ \mu = 6x+1;\ x = 0,\ \pm 1,\ \ \pm 2,\ \ \pm 3, \ldots. \tag{11}$$

where M_μ a harmonic term, representing the MMF amplitude of each harmonic p, refers to the total number of poles. It can be illustrated through the equation that besides the fundamental MMF there exist MMF waves of, i.e., *5p, 7p, 11p…n* pole pairs.

The stator winding is not a simple coil, but it consists of a number of identical coils that are placed in a distributive manner with certain angular coordinates as

$$W_{ss}(\theta) = \begin{cases} W_{ss} \cdot \left(1 - \dfrac{a}{2\pi}\right), & \theta_1 \le \theta \le \theta_2 \\ -W_{ss} \cdot \dfrac{a}{2\pi}, & \text{for other } \theta \end{cases} \tag{12}$$

W_{ss} is the slot conductors and a is a pitch.

http://dx.doi.org/10.5772/67245

4.2. Analytical expression of rotor MMF

The winding function of stator MMF is nothing else but MMF per unit current. In further text, the concept of stator MMF could be alternatively utilized to derive an expression for rotor MMF. Let us consider the rotor bars as a slot conductor and the end rings of the rotor will form a coil. Consequently, the combination of rotor bars with closed end ring forms coils at the rotor side:

$$W_{RR}(\theta) = \begin{cases} \left(1 - \frac{1}{R}\right), & -\frac{\pi}{R} \le \theta \le \frac{\pi}{R} \\ \frac{1}{R}, & \text{for other } \theta_R \end{cases} \tag{13}$$

The expression for rotor winding function can be derived by introducing Fourier series over the function in Eq. (13).

$$f(x) = a_0 + \sum_{n=1}^{\infty} (a_n \cos nx + b_n \sin nx) \tag{14}$$

$$W_{RR}(\theta_R) = \sum_{x=1}^{\infty} \frac{2}{x\pi} \sin\left(x\frac{\pi}{R}\right) \cos(x\theta_R) \tag{15}$$

Thus, following expression is achieved for rotor MMF:

$$F_{RR}(t, \theta_R) = \sum_{x=1}^{\infty} \frac{2}{x\pi} \sin\left(x\frac{\pi}{R}\right) \cos(x\theta_R) I_R \cos(s\omega t) \tag{16}$$

Apply product formula:

$$F_{RR1}(t, \theta_R) = \sum_{x=1}^{\infty} K_{\mu x} [\cos(s\omega t + x\theta_R) + \cos(s\omega t - x\theta_R)] \tag{17}$$

Referring to Eq. (11), it is clear that besides fundamental MMF there exist MMFs due to additional waves with $5p$, $7p$, $11p$,…, n. Consequently, the MMF of the rotor will also exit due to additional waves with $5p$, $7p$, $11p$. Further, **Figure 5** shows test rig designed to experimentally validate and capture MMF of induction motor. The test rig consists of 0.25 kW three-phase induction motor with 2 poles, 28 stator slots, and 30 rotor slots. While the spectrum of MMF is captured through PASPORT magnetic field sensor connected to PC through PASCO interface. The advantage of using PASPORT magnetic field sensor is that it offers very high sensitivity and is capable of monitoring the signal from −1000 to +1000 G as shown in **Figure 6**.

Figure 7 shows MMF spectrum against different harmonics, i.e., μ = 1,5,7,11, *and* 13 with corresponding μp = 2,10,14,22, *and* 26. It is more obvious that the additional harmonics waves will depend on the rotor bars and number of poles. Thus, besides the fundamental harmonic, rotor as well as stator MMF will exit for higher space harmonics. The abovementioned series of MMF due to μ harmonic term which could be defined as

Figure 5. Test rig for measuring MMF.

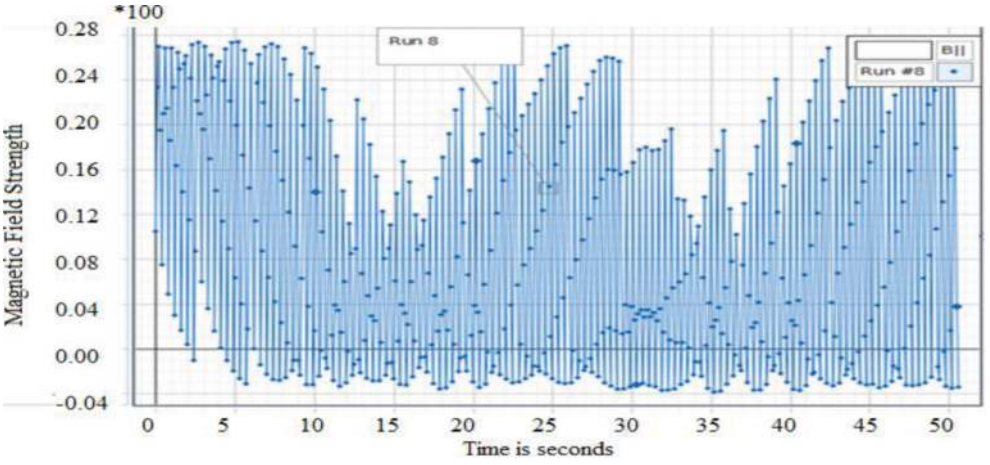

Figure 6. Spectrum of MMF two-axis magnetic field sensor.

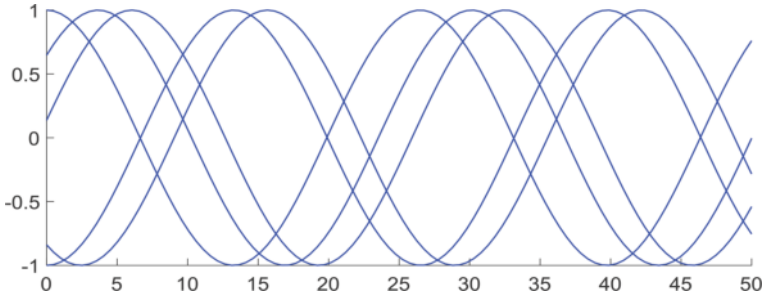

Figure 7. MMF at an instant ($p = 2$, $R = 30$, $\mu = 1$, 5, and 7).

http://dx.doi.org/10.5772/67245

$$\mu = 6u + 1;\ u = 0,\ \pm 1,\ \ \pm 2,\ \ \pm 3, \ldots.$$

The higher order harmonics are the consequence of the generation of rotor MMF. Due to analytical and experimental analysis, in this research work, an additional harmonic term "μ" is introduced to a rotor MMF. The rotor loops are $2\pi/R$ apart from each other with a phase shift of $\mu.p.2\pi/R$,; therefore, the frequency and the magnitude of the current will be same. The MMF in the consecutive rotor loop will be

$$F_{RR2}(t, \theta_R) = \sum_{x=1}^{\infty} K_{\mu x}\left[\cos\left(s\omega t + x\theta_R - (x + \mu p)\frac{2\pi}{R}\right) + \cos\left(s\omega t - x\theta_R + (x - \mu p)\frac{2\pi}{R}\right)\right] \tag{18}$$

The resultant MMF of the rotor will be the resultant of all the rotor loops along with all the harmonics.

$$F_R(t, \theta_R) = \sum_{j=0}^{R-1}\sum_{x=1}^{\infty} K_{\mu x}\left[\cos\left(s\omega t + x\theta_R - j.(x + \mu p)\frac{2\pi}{R}\right) + \cos\left(s\omega t - x\theta_R + j.(x - \mu p)\frac{2\pi}{R}\right)\right] \tag{19}$$

The harmonics in the rotor is due to fundamental and waves with $5p$, $7p$, $11p$, …, n poles. Moreover, from Eq. (19) through inspection, it is found that more prominent MMF waves exist if $x = \pm\mu p$ as well as $x = \pm lR + \mu p$ or $x = \pm lR - \mu p$ where, $l = 1, 2, 3\ldots$. Suppose if it is stated that x should be a positive integer, then MMF waves only exist for higher order harmonics, i.e., $x = |\pm\ \mu p|$, $x = |\pm lR + \mu p|$ and $x = \pm lR - \mu p$. Thus, for each of these waves in addition to fundamental MMF $x = |\pm\ \mu p|$, there are rotor harmonics at $x = |\pm lR + \mu p|$ with respect to the waves with 5p, $7p$, $11p$, …*poles*. If these MMFs are observed from stator side, they will have the following expression:

$$F_{ss}(t, \theta_R) = F_{ssF}(t, \theta_s) + F_{ssRH}(t, \theta_s) + F_{ssRH}(t, \theta_s) \tag{20}$$

$$F_{ss}(t, \theta_s) = M_{\mu}\cos(\omega t - \mu p\theta_s) \tag{21}$$

$$F_{ssRH}(t, \theta_s) = M_{\mu}\cos\left(\left(1 - \frac{lR}{P}(1 - s)\right)\omega t + (lR - \mu p)\theta_s\right) \tag{22}$$

$$F_{ssRH}(t, \theta_s) = M_{\mu}\cos\left(\left(1 + \frac{lR}{P}(1 - s)\right)\omega t - (lR + \mu p)\theta_s\right) \tag{23}$$

To validate and justify aforementioned discussion, the spectrum of MMF is obtained against harmonics of (*μ = 1, 5, and 7*) with respect to wave with $5p$, $7p$, $11p$, …*poles*. From **Figure 8**, it is obvious that against fundamental wave with, i.e., μ = 1, there will be rotor harmonics of order $R - \mu P$, $R + \mu P$, $2R - \mu P$, and $2R + \mu P$, i.e., 8th, 32th, 58th, and 68th as shown in **Figure 8**(a). For μ = 5, the rotor harmonic of order 20th, 40th, 50th, and 70th are shown in **Figure 8**(b). Similarly, for μ = 7 and rotor harmonic are of order 16th, 44th, 46th, and 74th as shown in **Figure 8**(c). Similarly, the MMF at the stator side will exit for $5p$, $7p$, $11p$,…. Further, this rotor harmonic will be useful to diagnose the faults.

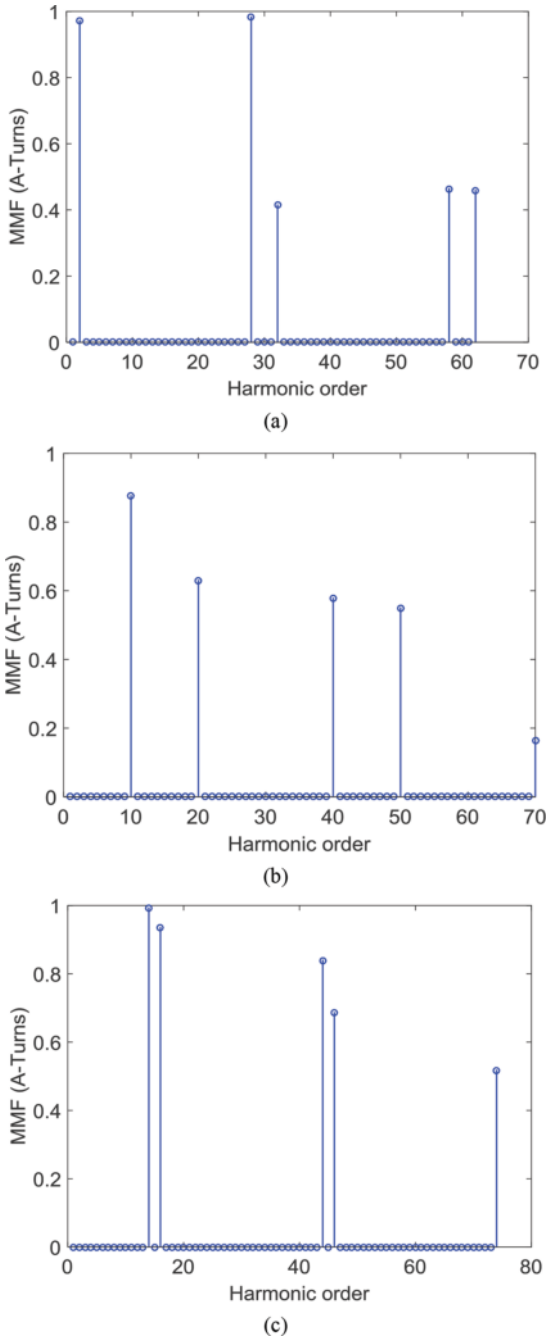

Figure 8. Harmonic order of MMF ($p = 2$, $R = 30$, $\mu = 1$, 5, and 7).

http://dx.doi.org/10.5772/67245

4.3. Analysis of unbalanced voltage and its effect on MMF

As mentioned earlier, unbalanced voltage supply is one of the major sources of stator winding failure. Under unbalanced voltage, the symmetry of induction motor is disturbed and the effect of unbalanced voltage is equivalent to negative sequence voltage. Motor acts as two different motors, one for the positive sequence and the other for the negative sequence. Each set of the sequence will produce corresponding balanced currents and the synthesis of the two sets of current is an actual current produced by the original unbalanced voltages. The response of a motor to the positive sequence voltage is the same as for normal voltage. However, the negative sequence currents set up a reverse MMF, so if a slip of a motor is (s) with respect to the positive sequence field, it will be (2-s) relative to the negative sequence MMF. Moreover, a motor behaves as two separate motors, one running at slip (s) with a terminal voltage while the other running with a slip of (2-s).

5. Fault diagnosis system through experimental results

For a reliable fault diagnostic method, it is essential to have a good understanding of the motor response for healthy and faulty conditions. To eliminate additional cost for monitoring scheme, it is important to find out the fault through current signature. The current signature can be easily measured and are most sensitive to any fault. Moreover, the cost of current monitoring is not imposed on the system because in every industry the current sensors are embedded. Thus, in proposed work, two methods are proposed to diagnose unbalanced voltage. In the first method, unbalanced voltage is diagnosed through an efficient MCSA technique. Due to the rapid complexity in industrial plants, it is inconceivable to continue human inspection to diagnose the faults. Consequently, to avoid human inspection, in addition to MCSA, AI-based ANN high performance fully automated method is proposed.

5.1. Diagnosis of unbalanced voltage through harmonic component

It is reported that MCSA is a noninvasive and an economically most suitable method to diagnose motor faults. Thus, the basis of MCSA is of fundamental importance to diagnose unbalanced voltage supply. Asymmetry in the power supply will generate negative sequence current that will produce a backward rotating field at double slip frequency with respect to the forward rotating rotor. The MMF that is caused by both the fields will induce voltage and current at the stator side, and the effect of this current will be more prominent at newly introduced rotor harmonic frequency given as

$$f_{RH} = \left[1/2\left(k\frac{2N_r}{P}\right)(1-s) \pm 1\right]F_s,\ k = 1, 2, 3\ldots\ldots\ldots \tag{24}$$

where, N_r and p represent rotor bars and poles, respectively, while s and F_s are the slip and applied frequency, respectively. It can be analyzed through modified expression of rotor harmonic that spectral content of current will be more prominent at these frequencies.

5.2. Experimental diagnosis of unbalanced voltage

To validate the proposed methods at an incipient stage, experimental data and justification are required. For this purpose, a number of experiments are carried on the induction motor. The motor is assembled and designed in electrical machine lab to study the behavior of the motor under different degree of unbalanced voltage in a single phase.

The block diagram and a testbed are shown in **Figures 9** and **10**, which are composed of a three-phase squirrel cage induction motor connected in star layout with, two pole pairs, variable adjustable voltage. The variation in the voltage supply is achieved through Lab-Voltage variable Power supply model 8821-2A. For data acquisition, FLUKE interface and PC are used. **Table 1** shows the rated specification of the motor that is used for an experiment, while **Table 2** shows the percentage unbalanced voltage that is introduced through variable Power supply model 8821-2A.

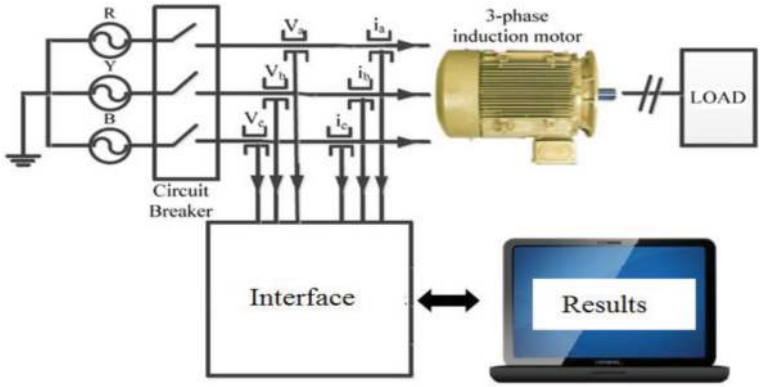

Figure 9. Test rig.

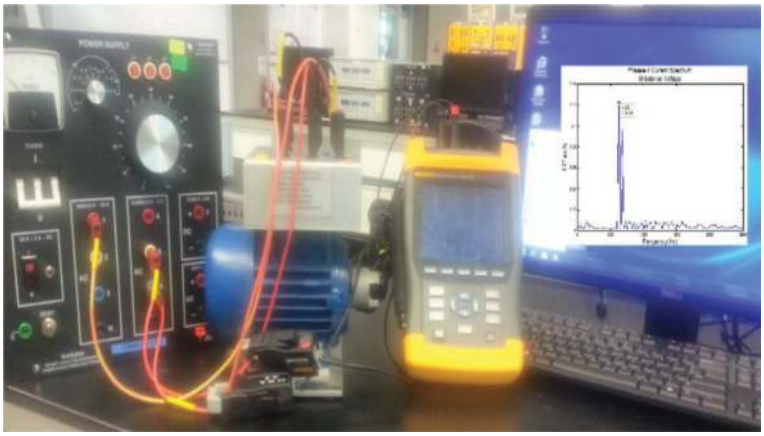

Figure 10. Experimental setup.

http://dx.doi.org/10.5772/67245

Motor feature	
Motor type	Three-phase induction motor
Balanced line voltage (*V*)	415
Synchronous speed (rpm)	3000
Rated speed (rpm)	2700
Motor slip	0.1
Power (W)	250
Frequency (Hz)	50
Poles	2
Stator slots	24
Rotor slots	22

Table 1. Rated values of induction motor.

	Voltage phase_1 (V)	Voltage phase _2 (V)	Voltage phase _3 (V)	% total voltage unbalanced
Balanced voltage	415	415	415	0
Unbalanced voltage	415	415	385	7.5
Unbalanced voltage	415	415	355	15
Unbalanced voltage	415	415	335	21

Table 2. Asymmetry in voltage supply.

Figure 11 shows the experimental results of current signature of three-phase induction motor supplied with a perfectly balanced voltage source. Referring to analytical expression (24), from the current spectrum, it is obvious that the current harmonics components at 450 and 550 Hz are due to induced EMF. It can easily be seen that the new series of rotor harmonic are the most prominent in the current spectrum. Hence, these frequency components in the current spectrum can be selected as yardsticks to measure the effects of unbalanced voltage.

To investigate the effect of unbalanced voltage, the percentage unbalanced in a single phase of an induction motor is varied through Lab-Voltage variable Power supply model 8821-2A. Further, the system response is analyzed through a new series of rotor harmonic. It is obvious from **Figures 12–14** that show that with the variation in the voltage supply there is a significant variation in the amplitude of the harmonic component at 450 and 550 Hz. It is also apparent that the amplitude of these harmonic is directly proportional to the degree of unbalanced voltage. Thus, the increase in the degree of unbalanced voltage will significantly increase the harmonic components at 45 and 550 Hz. Unbalanced voltage supply has drastic consequences on the motor operation because it can lead the current 6–10 times higher than the nominal rate. The increase in current will be much severed for the winding because even a 10% increase in temperature damages half of the winding insulation and results in short circuit. Thus, the proposed method will be a more appropriate and noninvasive technique to diagnose unbalanced voltage supply at in incipient stage and avoid catastrophic failure.

5.3. Results and discussions

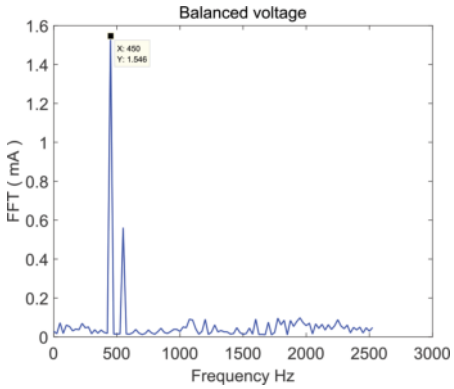

Figure 11. Balanced voltage.

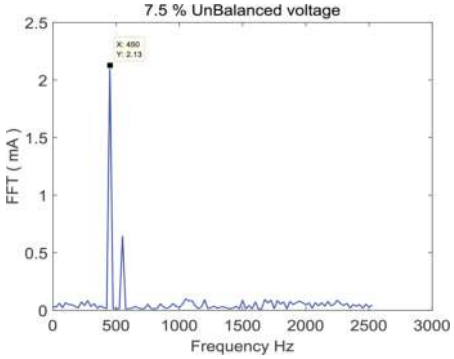

Figure 12. 7.5% Unbalanced voltage.

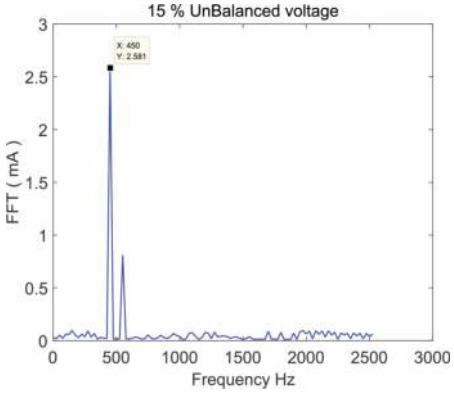

Figure 13. 15% Unbalanced voltage.

http://dx.doi.org/10.5772/67245

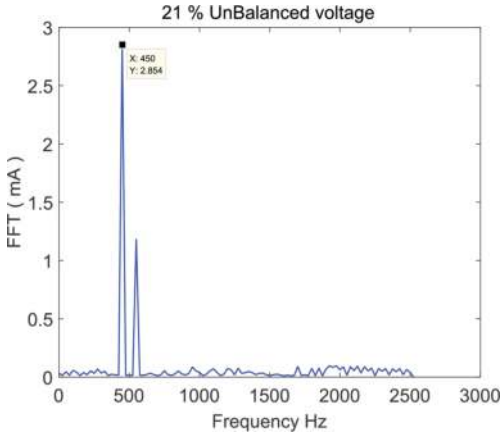

Figure 14. 21% Unbalanced voltage.

6. Fully automated detection of unbalanced voltage

6.1. ANN classifier design

The recognition of the pattern has been a key factor in the growth of fault diagnosis methods. Over the last few decades, automated techniques adopting the ANN have attracted the researchers due to excellent innovation in various industrial applications such as aerospace, pneumatic, chemical, and renewable energy. Similarly, in an electrical field, a major part of the research has been conducted on parameters such as identification in control systems, power system, and particularly detection of induction motor faults. The ANN is most feasible and reliable approach because these techniques are less model dependent of the process and in their generalization capacity. Moreover, ANN provides interpretation of real-time tracking by accommodating variation in the learning data. This efficiency is dependent on the choice of the data that are selected as inputs representing the defects. Hence, the ultimate obligation for effective implementation of ANN to diagnose the exact fault is the availability of relevant rich statistics that are identified as an input data for each fault. Therefore, it is compulsory that the input data of ANN should be meaningful indicators of the faults. Selection of such a data set is not an easy task. However, a convenient way is to select the parameter as a fault indicator that gives the most information about the fault and discard the rest [30]. In this work, feed-forward multilayer perceptron (MLP) ANN is used while the ANN is trained by the back-propagation (BP) algorithm.

6.2. Description of the proposed method

The choice of eccentricity harmonic detection, which increases the discernment between healthy and faulty motor, is of great interest that most of the researchers look for. From experimental results, most of the researchers confronted with the fact that the amplitude of third-order harmonic was considered alone distinction criterion between the healthy and

unbalanced voltage source, which is not sufficient owing the unbalanced condition because the third-order harmonic also exits for a perfect balanced source. In proposed work, the main focus is to use ANN technique in such a way that it is able to identify and declare healthy or faulty condition after reception of each data set. To acquire the desired results, certain stages must be carried out such as relevant input variables, output variables, and layers and neurons in each layer as shown in **Figure 15**.

The proposed method is based on the current signature of an induction motor. From the current signature, two indicators of voltage unbalanced are extracted, i.e., (I-1, I-2) based on new series of rotor harmonic (Eq. (20)). As shown in **Figure 16**, these indicators are fed to the ANN for automatic fault detection. The computation of this input is performed as illustrated in **Figure 16**. Initially, fast Fourier transformer (FFT) is performed at line currents to extract the magnitude and the phase angle of each line current. After that, the magnitude and phases of certain harmonic components are extracted and fed to ANN. Accordingly, the used multilayer feed-forward neural network with two input and four outputs is depicted in **Figure 16** with:

I-1: The magnitude of new series of rotor harmonic.

I-2: The phase angle of new series of rotor harmonic.

The neural network approach to diagnose unbalanced voltage is carried out in two phases, i.e., training and testing. In the first phase known as training phase, the ANN is automated trained to capture the underlying relations among inputs and desired outputs. While in the second phase the results are computed through ANN testing, the data set used for testing is random,

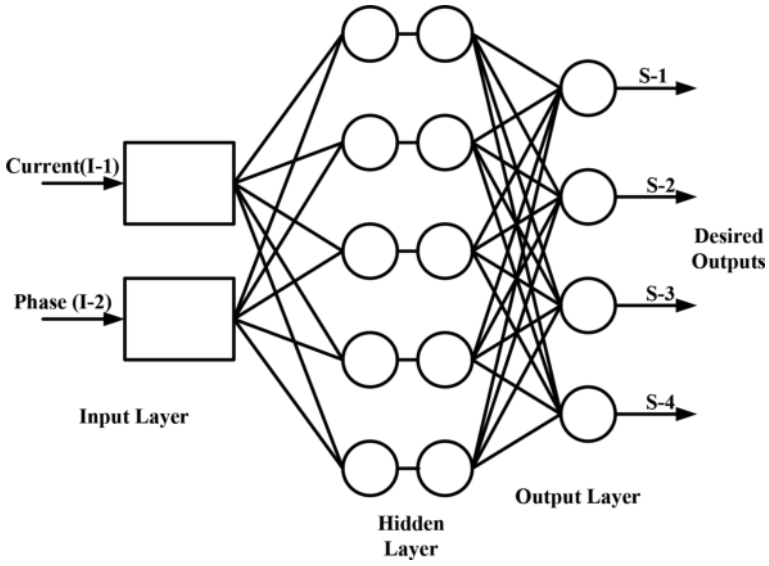

Figure 15. ANN architecture.

http://dx.doi.org/10.5772/67245

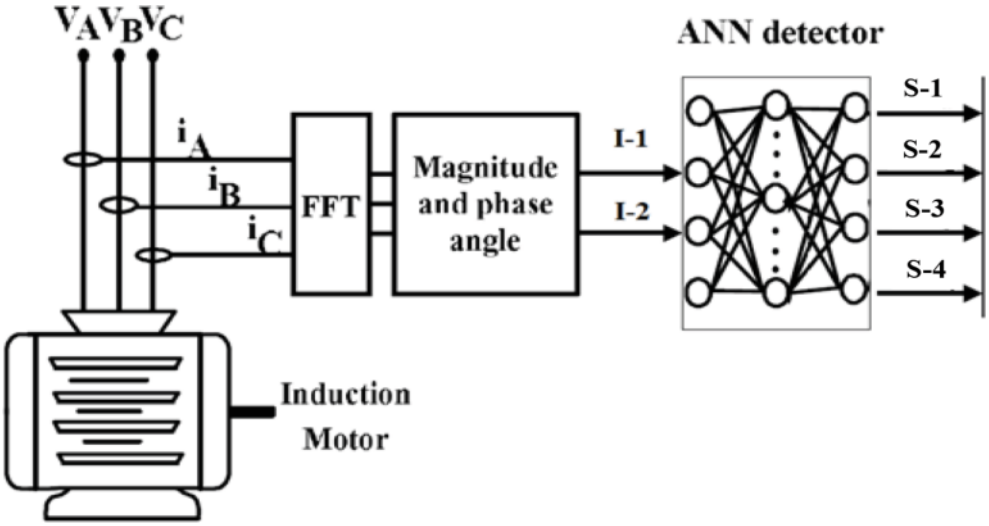

Figure 16. Model of proposed ANN multilayer feed-forward neural network.

which is not used before to check the efficiency of ANN. Note that in this proposed work, experimental data are collected for the testbed designed in electrical machine lab. The variation in the voltage supply is achieved through Lab-Voltage variable Power supply model 8821-2A.

6.3. Experimental results of the proposed ANN technique

6.3.1. Testbed description

To validate the proposed methods, experiments are carried on the induction motor. The testbed is shown in **Figure 10**, and its parameters are listed in **Table 1**. The variation in the voltage supply is achieved through Lab-Voltage variable Power supply model 8821-2A. For data acquisition, FLUKE interface and Intel (R) Xeon (R) computer having CPU E5-1650V2@3.50GHz, 64 GB RAM, and 64-bit operating system are used. Furthermore, for data acquisition, these analogy sensors are connected to PC through FLUKE interface. A total of 2040 samples of data for each class from FLUKE interface are interpreted by MATLAB (R2015a) software in order to compute the desired harmonics and the phase shift of each phase. This task is carried out through developed algorithm and the achievement of the fault diagnosis task by the NN.

In this research, different sequences of tests are conducted on the motor. The results of these tests are the basis to carry-out the next two phases of fault detection technique, i.e., training and the test phase, in order to experimentally validate the performance of the NN. The tests are conducted by configuring degree of unbalanced voltage in phase-C, for the following variations:

1. All the three phases are perfectly balanced.
2. Phase-C with 7.5% of unbalanced voltage while other two phases with nominal voltage.
3. Phase-C with 15% of unbalanced voltage while other two phases with nominal voltage.
4. Phase-C with 21% of unbalanced voltage while other two phases with nominal voltage.

6.3.2. Experimental characteristics of new series of harmonic

The plot in **Figures 17–19** illustrates the experimental characteristics in a new series of rotor harmonic for unbalanced voltage, respectively, with increasing degree of the unbalanced voltage of 7.5, 15, and 21%. It is obvious from the experimental computed result that there is a direct impact of unbalanced voltage on the amplitude of new rotor harmonics. With increasing unbalanced voltage, there is a direct increase in the amplitude of new series of harmonics in phase-A and phase-B, while there is a decrease in the amplitude of phase-C, which reflects that the unbalanced is in phase-C. Despite the difference in values, the evolution in the amplitude of plotted curves against increasing percentage of unbalanced voltage is an indicator to the permutation in the increasing degree of unbalanced voltage.

6.3.3. Training results

A number of input and output data set are processed during the learning phase. Thus, a series of training data set is fed to the ANN. The training data is extracted from the current signature and the targeted input database (I-i) with corresponding output database (S-i). The input data set of training is composed of different degree of unbalanced voltage. Each training data set is represented by input and output vectors, i.e., [I-1, I-2] = [S-1, S-2, S-3, S-4].

Total training input data set consists of 80 successive sequences of 20 examples to balanced voltage, 20 examples of 7.5% of unbalanced voltage, 20 examples of 15% of unbalanced

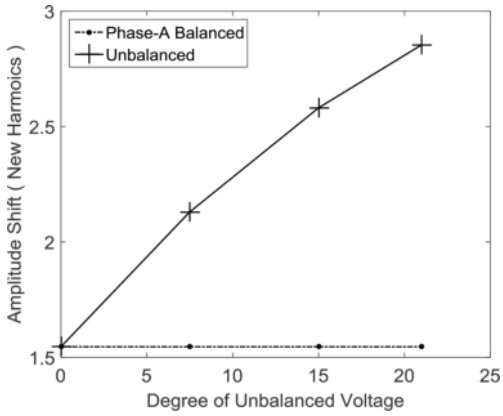

Figure 17. Characteristic of new harmonic on phase-A.

http://dx.doi.org/10.5772/67245

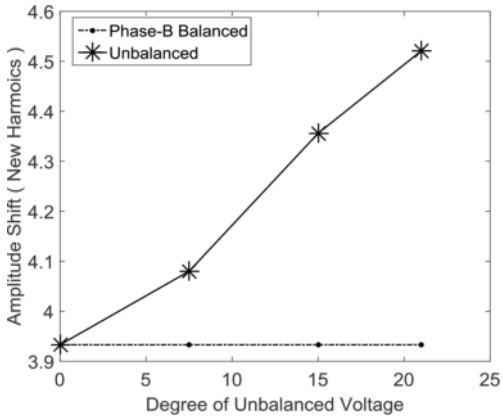

Figure 18. Characteristic of new harmonic on phase-B.

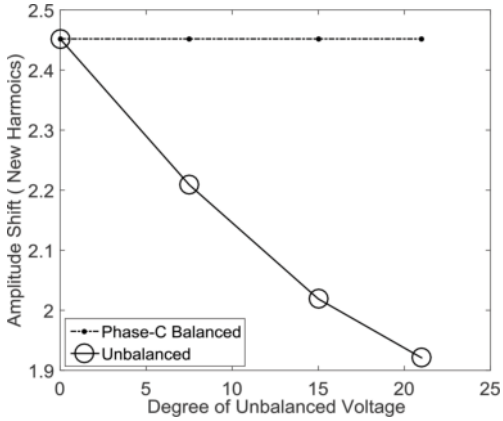

Figure 19. Characteristic of new harmonic on phase-C.

voltage, and 20 examples of 21% of unbalanced voltage in phase-C of an induction motor. The training output data are arranged in order to accomplish desired outputs (S-i) using a logical expression, i.e., (0 and 1) to identify the condition of the motor as follows:

S-1 = 1 All the three phases are perfectly balance; otherwise, S-1 = 0.

S-2 = 1 Phase-C with 7.5% of unbalanced voltage while other two phases with nominal voltage; otherwise, S-2 = 0.

S-3 = 1 Phase-C with 15% of unbalanced voltage while other two phases with nominal voltage; otherwise, S-3 = 0.

S-4 = 1 Phase-C with 21% of unbalanced voltage while other two phases with nominal voltage otherwise, S-4 = 0.

To elucidate the state, the outputs (S-1, S-2, S-3, S-4) are set to:

[0, 0, 0] All the three phases are perfectly balance.

[1, 0, 0] Phase-C with 7.5% of unbalanced voltage.

[0, 1, 0] Phase-C with 15% of unbalanced voltage.

[0, 0, 1] Phase-C with 21% of unbalanced voltage.

The total training input data set consists of 80 successive sequences of 20 examples to balanced voltage, 20 examples of 7.5% of unbalanced voltage, 20 examples of 15% of unbalanced voltage, and 20 examples of 21% of unbalanced voltage in phase-C of an induction motor. Using the NN structure with two inputs, four outputs, and 10 hidden neurons, as shown in **Figure 16**, the classifier is trained on the experimental data shown in **Figures 17–19**. It is obvious that satisfactory training results are achieved. From **Figure 20**, it can be perceived that mean squared error (MSE) reached to 4.63×10^{-09} after 1000 epochs. The corresponding MSE shows that successful classification is accomplished with low errors.

6.3.4. Test results

The objective of test results is to evaluate the feasibility and accuracy of the NN. Thus, to test the performance of proposed method, random and successive range of data is fed to ANN classifier with 20 examples of each case. From the MSE results, it can be analyzed that error is very low, and this is the indication that the proposed ANN model has correctly classified all the classes. Usually, the classifier performance is evaluated by estimating its generalization error. However, in many cases the low value of error is not enough to judge and ensure that the features were correctly learnt because too low error can also refer that the network has over fitted the data [31].

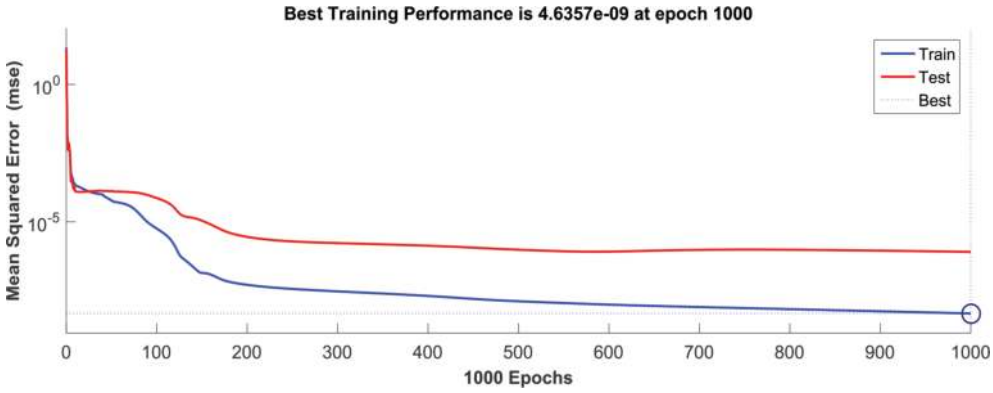

Figure 20. Performance of proposed ANN.

http://dx.doi.org/10.5772/67245

To properly classify the network performance Receiver Operating Characteristic (ROC) and confusion matrix are presented in this work. The ROC curve is a two-dimensional measurement that represents the classifier performance rate. It expresses the probability rate of corrected samples classified versus misclassified ones. In practice, ROC curve shows performance of proposed method through area under the curve. The performance

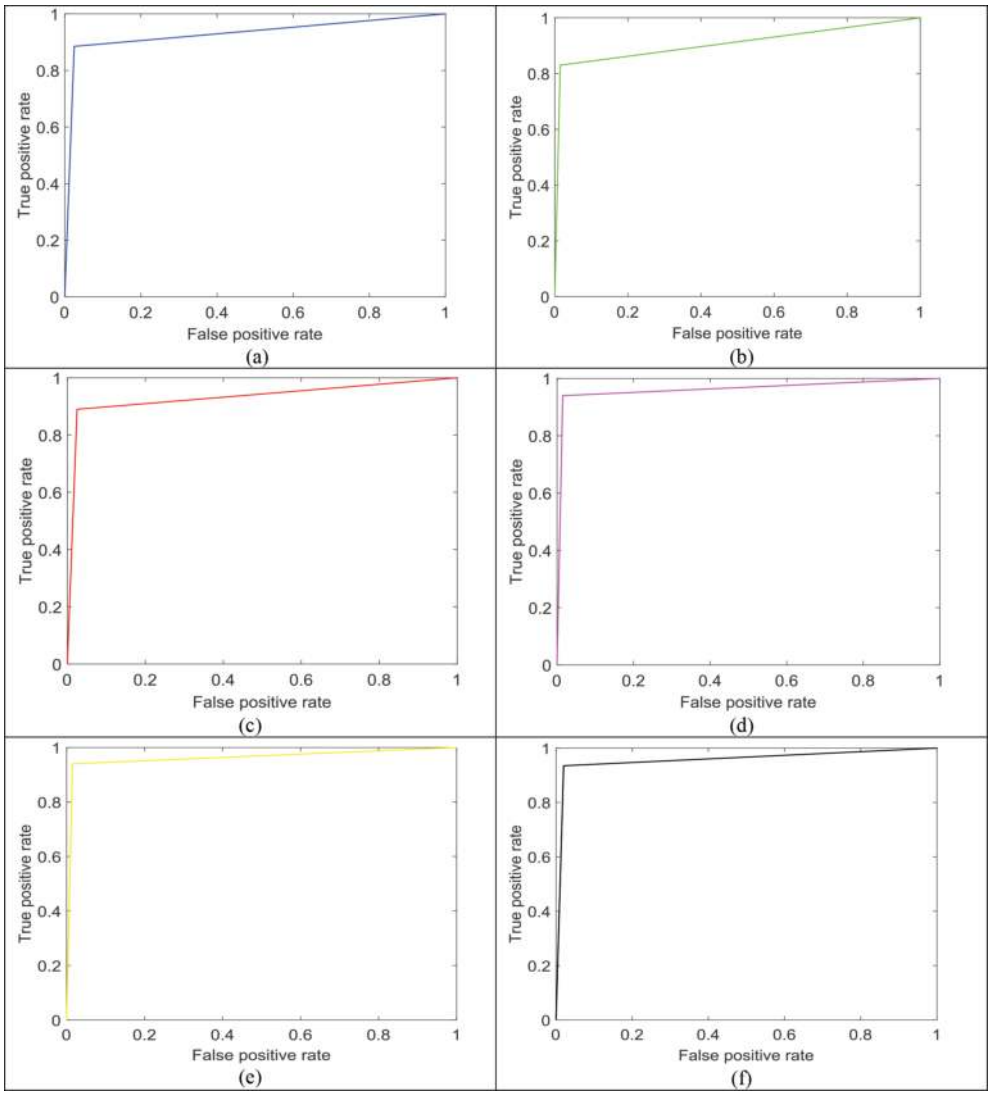

Figure 21. ROC curve w.r.t. (a) balanced-unbalanced 7.5%, (b) balanced-unbalanced 15%, (c) balanced-unbalanced 21%, (d) unbalanced 7.5%-unbalanced 15%, (e) unbalanced 7.5%-unbalanced 21%, (f) unbalanced 15%-unbalanced 21%.

of the network depends on the trade-off between robustness and sensitivity. The robustness and sensitivity of proposed techniques can be discovered through a series of experiments. ROC curve is carried out to detect and evaluate the proposed methodology that how efficiently propose technique diagnoses the level of unbalanced voltage supply. The ROC curve can be evaluated for each class to extract the performance against that particular class. From **Figure 21**, the ROC graph shows the trade-off between the probabilities of true positives rate (tpr) versus the probability of false positives rate (fpr). From ROC curve of each class, it can be seen that for all the classes the curve is closer to the top left corner which demonstrate that area under the curve is higher and the proposed method has efficiently diagnosed the level of unbalanced voltage supply. Mathematically, tpr and fpr can be expressed as

$$tpr = \frac{\text{true positives}}{\text{true positives} + \text{false negatives}} \tag{25}$$

$$fpr = \frac{\text{false positives}}{\text{false positives} + \text{true negatives}} \tag{26}$$

Further, confusion matrix is constructed of each class to report the performance of a classifier. In **Table 3**, a confusion matrix is presented with dimension defined by the number and the type of classes. For clarification, the headings pointed out in confusion matrix of **Table 3** are defined as follows: 0 ≡ balanced voltage supply, 1 ≡ 7.5% unbalanced voltage supply, 2 ≡ 15% unbalanced

		Predicted 0	Predicted 1
Actual	0	16	4
	1	0	20

(a)

		Predicted 0	Predicted 2
Actual	0	16	4
	2	2	18

(b)

		Predicted 0	Predicted 3
Actual	0	18	2
	3	2	18

(c)

		Predicted 1	Predicted 2
Actual	1	20	0
	2	2	18

(d)

		Predicted 1	Predicted 3
Actual	1	20	0
	3	2	18

(e)

		Predicted 2	Predicted 3
Actual	2	20	0
	3	2	18

(f)

Table 3. Confusion matrix of (a) balanced-unbalanced 7.5%, (b) balanced-unbalanced 15%, (c) balanced-unbalanced 21%, (d) unbalanced 7.5%-unbalanced 15%, (e) unbalanced 7.5%-unbalanced 21%, (f) unbalanced 15%-unbalanced 21%.

http://dx.doi.org/10.5772/67245

voltage supply, and 3 ≡ 21% unbalanced voltage supply. The percentage of proper or correct identification of unbalanced voltage is represented in the major diagonal, while the out of major diagonal represents the errors (means the confusion) among the various classes. The results of confusion matrix demonstrate high degree of accuracy that shows that the classification associated with the use of proposed method is reliable to diagnose and distinguish between different levels of unbalanced voltage supply. The overall accuracy of proposed model is 85%, which is a big achievement.

The synthesis of the proposed work helps to conclude the feasibility and efficiency through the accuracy of the result that how close the ANN results are to the actual results. In this work, it is illustrated through experimental and classifier work that how accurate the proposed method is in locating the degree of unbalanced voltage. Moreover, the proposed method is robust and can be suggested to demonstrate the health of any motor.

7. Conclusion and future directions

As in recent era, the majority of induction motor fault diagnosis techniques are essentially noninvasive (online) to ensure continue production, reliability, and consequently. Therefore, in this chapter, a comprehensive analysis of noninvasive techniques is carried out, which are used to diagnose stator winding failure. Further, this chapter presents derivation by utilizing winding function approach to find out the conductor segments responsible for the generation of MMF. The knowledge of induced voltage at stator winding through MMF helps to propose a new noninvasive regime in order to diagnose unbalanced voltage. Thus, a new series of rotor harmonics are introduced and one can easily observe the performance through a graph that the amplitude of higher order harmonics increases against the various level of unbalanced voltage. Due to the rapid complexity in industrial plants, it is inconceivable to continue human inspection to diagnose the faults. Thus, to avoid human inspection, in additional to new series of rotor harmonic, a fully automatic method based on a neural network is proposed to diagnose unbalanced voltage at an incipient stage. The diagnostic process of ANN is fully automated; it can be observed through the pattern or the trend of ANN graphs that there is a significant rise in the new series of current harmonic. Further, through ROC curve, confusion matrix and overall accuracy of proposed method show that the novel features extraction are more reliable for diagnosing the fault. The classification tasks of proposed automated noninvasive method not only diagnoses unbalanced voltage but it also distinguishes between various levels of unbalanced voltage, which reflects the effectiveness and reliability of the proposed diagnosis process. The scope of this research can readily be extended to identify and locate the exact unbalanced voltage phase through a current spectrum. In proposed method, the features are extracted through the current harmonics, while the research can be extended to extract the unbalanced features through phase shift.

Author details

Muhammad Aman Sheikh[1]*, Nursyarizal Mohd Nor[1], Taib Ibrahim[1], Sheikh Tahir Bakhsh[2], Muhammad Irfan[3] and Hanita Binti Daud[4]

*Address all correspondence to: amanatd88@yahoo.com

1 Department of Electrical & Electronic Engineering, Universiti Teknologi Petronas, Bandar Seri Iskandar, Malaysia

2 Computer Science Department, Faculty of Computing and Information Technology, King Abdul Aziz University, Jeddah, Kingdom of Saudi Arabia

3 Electrical Engineering Department, Faculty of Engineering, Najran University, Kingdom of Saudi Arabia

4 Department of Fundamental & Applied Sciences, Universiti Teknologi Petronas, Bandar Seri Iskandar, Malaysia

References

[1] M. Irfan, N. Saad, R. Ibrahim, V. S. Asirvadam, N. Hung, and M. A. Magzoub, "Analysis of bearing surface roughness defects in induction motors," *Journal of Failure Analysis and Prevention*, vol. 15, pp. 730–736, 2015.

[2] M. Irfan, N. Saad, R. Ibrahim, and V. Asirvadam, "An on-line condition monitoring system for induction motors via instantaneous power analysis," *Journal of Mechanical Science and Technology*, vol. 29, pp. 1483–1492, 2015.

[3] W. Thomson, "A review of on-line condition monitoring techniques for three-phase squirrel-cage induction motors-past present and future," in *Keynote address at IEEE symposium on diagnostics for electrical machines, power electronics and drives, Gijon, Spain*, 1999, pp. 3–18.

[4] W. T. Thomson and M. Fenger, "Current signature analysis to detect induction motor faults," *Industry Applications Magazine, IEEE*, vol. 7, pp. 26–34, 2001.

[5] S. Nandi, S. Ahmed, and H. A. Toliyat, "Detection of rotor slot and other eccentricity related harmonics in a three phase induction motor with different rotor cages," *Energy Conversion, IEEE Transactions on*, vol. 16, pp. 253–260, 2001.

[6] H. A. Toliyat and N. A. Al-Nuaim, "Simulation and detection of dynamic air-gap eccentricity in salient pole synchronous machines," in *Industry Applications Conference, 1997. Thirty-Second IAS Annual Meeting, IAS'97., Conference Record of the 1997 IEEE*, 1997, pp. 255–262.

http://dx.doi.org/10.5772/67245

[7] M. E. H. Benbouzid, M. Vieira, and C. Theys, "Induction motors' faults detection and localization using stator current advanced signal processing techniques," *IEEE Transactions on Power Electronics*, vol. 14, pp. 14–22, 1999.

[8] A. Siddique, G. Yadava, and B. Singh, "A review of stator fault monitoring techniques of induction motors," *Energy conversion, IEEE Transactions on*, vol. 20, pp. 106–114, 2005.

[9] G. Acosta, C. Verucchi, and E. Gelso, "A current monitoring system for diagnosing electrical failures in induction motors," *Mechanical Systems and Signal Processing*, vol. 20, pp. 953–965, 2006.

[10] J. Jee-Hoon, J.-J. Lee, and K. Bong-Hwan, "Online Diagnosis of Induction Motors Using MCSA," *IEEE Transactions on Industrial Electronics*, vol. 53, pp. 1842–1852, 2006.

[11] S. Nandi and H. A. Toliyat, "Novel frequency domain based technique to detect incipient stator inter-turn faults in induction machines," in *Industry Applications Conference, 2000. Conference Record of the 2000 IEEE*, 2000, pp. 367–374.

[12] M. Eltabach, J. Antoni, and M. Najjar, "Quantitative analysis of noninvasive diagnostic procedures for induction motor drives," *Mechanical Systems and Signal Processing*, vol. 21, pp. 2838–2856, 2007.

[13] N. Arthur and J. Penman, "Induction machine condition monitoring with higher order spectra," *IEEE Transactions on Industrial Electronics*, vol. 47, pp. 1031–1041, 2000.

[14] R. Isermann, "Model-based fault-detection and diagnosis–status and applications," *Annual Reviews in Control*, vol. 29, pp. 71–85, 2005.

[15] V. Uraikul, C. W. Chan, and P. Tontiwachwuthikul, "Artificial intelligence for monitoring and supervisory control of process systems," *Engineering Applications of Artificial Intelligence*, vol. 20, pp. 115–131, 2007.

[16] M. A. Awadallah and M. M. Morcos, "Application of AI tools in fault diagnosis of electrical machines and drives-an overview," *IEEE Transactions on Energy Conversion*, vol. 18, pp. 245–251, 2003.

[17] F. Filippetti, G. Franceschini, C. Tassoni, and P. Vas, "AI techniques in induction machines diagnosis including the speed ripple effect," *IEEE Transactions on Industry Applications*, vol. 34, pp. 98–108, 1998.

[18] A. Siddique, G. Yadava, and B. Singh, "Applications of artificial intelligence techniques for induction machine stator fault diagnostics: review," in *Diagnostics for Electric Machines, Power Electronics and Drives, 2003. SDEMPED 2003. 4th IEEE International Symposium on*, 2003, pp. 29–34.

[19] J. S. Hsu, "Monitoring of defects in induction motors through air-gap torque observation," *IEEE Transactions on Industry Applications*, vol. 31, pp. 1016–1021, 1995.

[20] M. Sahraoui, S. Zouzou, A. Ghoggal, and S. Guedidi, "A new method to detect inter-turn short-circuit in induction motors," in *2010 XIX International Conference on Electrical Machines (ICEM)*, 2010, pp. 1–6.

[21] S. M. A. Cruz and A. J. M. Cardoso, "Multiple reference frames theory: a new method for the diagnosis of stator faults in three-phase induction motors," *IEEE Transactions on Energy Conversion*, vol. 20, pp. 611–619, 2005.

[22] A. Ukil, S. Chen, and A. Andenna, "Detection of stator short circuit faults in three-phase induction motors using motor current zero crossing instants," *Electric Power Systems Research*, vol. 81, pp. 1036–1044, 2011.

[23] N. Mehla and R. Dahiya, "An approach of condition monitoring of induction motor using MCSA," *International Journal of Systems Applications, Engineering and Development*, vol. 1, pp. 13–17, 2007.

[24] J. Cusido, L. Romeral, J. A. Ortega, J. A. Rosero, and A. Garcia Espinosa, "Fault detection in induction machines using power spectral density in wavelet decomposition," *IEEE Transactions on Industrial Electronics*, vol. 55, pp. 633–643, 2008.

[25] S. B. Lee, R. M. Tallam, and T. G. Habetler, "A robust, on-line turn-fault detection technique for induction machines based on monitoring the sequence component impedance matrix," *IEEE Transactions on Power Electronics*, vol. 18, pp. 865–872, 2003.

[26] F. Villada, D. R. Cadavid, J. E. Aedo, B. A. Benavides, and E. Velilla, "The negative sequence impedance as fault indicator in induction motors," *Revista Facultad de Ingeniería*, pp. 7–13, 2013.

[27] S. Nandi and H. A. Toliyat, "Novel frequency-domain-based technique to detect stator interturn faults in induction machines using stator-induced voltages after switch-off," *IEEE Transactions on Industry Applications*, vol. 38, pp. 101–109, 2002.

[28] S. Nandi, "Detection of Stator Faults in Induction Machines using Residual Saturation Harmonics," in *2005 IEEE International Conference on Electric Machines and Drives*, 2005, pp. 256–263.

[29] P. Lamim, R. Pederiva, and J. Brito, "Detection of stator winding faults in induction machines using an internal flux sensor," in *Diagnostics for Electric Machines, Power Electronics and Drives, 2007. SDEMPED 2007. IEEE International Symposium on*, 2007, pp. 432–437.

[30] M. Bouzid, N. Bellaaj, K. Jelassi, G. Champenois, and L. Signac, "Location of an inter turns short-circuit fault in the stator windings of induction motor by neural network," 2007.

[31] Demian, C., Cirrincione, G., and Capolino, G. A. (2002, November) "A neural approach for the fault diagnostics in induction machines," in *IECON 28th Annual Conference of the IEEE Industrial Electronics Society,* (Vol. 4, pp. 3372–3376). IEEE.